NANO LETTERS

2007
Vol. 7, No. 2
525−530

Nanostructure Fabrication by Ultra-High-Resolution Environmental Scanning Electron Microscopy

Milos Toth,*,† Charlene J. Lobo,‡ W. Ralph Knowles,† Matthew R. Phillips,‡ Michael T. Postek,§ and András E. Vladár§

FEI Company, 29 Water Street #216-217, Newburyport, Massachusetts 01950, Microstructural Analysis Unit, University of Technology, Sydney, P.O. Box 123, Broadway, New South Wales 2007, Australia, and National Institute of Standards and Technology (NIST||), 100 Bureau Drive, Gaithersburg, Maryland 20899-8212

Received December 6, 2006; Revised Manuscript Received January 3, 2007

ABSTRACT

Electron beam induced deposition (EBID) is a maskless nanofabrication technique capable of surpassing the resolution limits of resist-based lithography. However, EBID fabrication of functional nanostructures is limited by beam spread in bulk substrates, substrate charging, and delocalized film growth around deposits. Here, we overcome these problems by using environmental scanning electron microscopy (ESEM) to perform EBID and etching while eliminating charging artifacts at the nanoscale. Nanostructure morphology is tailored by slimming of deposits by ESEM imaging in the presence of a gaseous etch precursor and by pre-etching small features into a deposit (using a stationary or a scanned electron beam) prior to a final imaging process. The utility of this process is demonstrated by slimming of nanowires deposited by EBID, by the fabrication of gaps (between 4 and 7 nm wide) in the wires, and by the removal of thin films surrounding such nanowires. ESEM imaging provides a direct view of the slimming process, yielding process resolution that is limited by ESEM image resolution (∼1 nm) and surface roughening occurring during etching.

Gas-mediated electron beam induced deposition (EBID) and etching (EBIE)[1−3] are promising maskless techniques for nanofabrication at sub-10-nm length scales. In EBID and EBIE, adsorbed precursor molecules are dissociated by electrons crossing the surface. These reactive dissociation products convert surface material to volatile or nonvolatile reaction products, giving rise to deposition or etching under an electron beam (Figure 1). Under extreme conditions, EBID has been used to produce nanodots with diameters close to 1 nm.[4,5] However, such high resolution has only been achieved using transmission electron microscopy (TEM), which requires the use of thin substrates that are unsuitable for most applications. Scanning electron microscopy (SEM) has been used to produce carbonaceous dots with diameters of approximately 4 nm using very short beam exposure times (similar to 200 μs) to cross-link residual hydrocarbons present on a Si substrate in a high vacuum environment.[6] However, in order to control both deposit composition and morphology, appropriate precursor gases must be injected into the SEM chamber, and long as well as short electron beam exposure times must be used. Under such conditions, minimum feature dimensions typically exceed 20 nm, and functionality is hindered by delocalized deposits grown unintentionally around EBID structures (e.g., thin films that give rise to

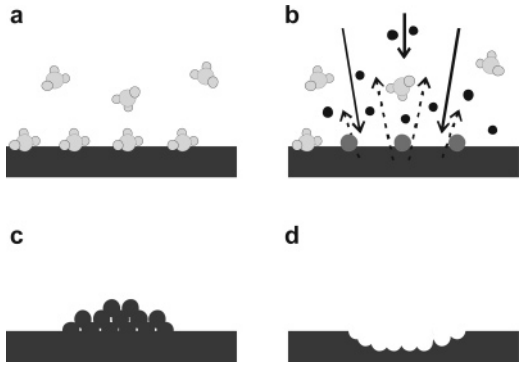

Figure 1. Simplified schematic of gas-mediated electron-beam-induced deposition (a−c) and etching (a, b, d): (a) precursor adsorption and surface diffusion; (b) dissociation induced by primary, backscattered, and secondary electrons; (c) deposition; (d) volatilization of surface material.

* Corresponding author. E-mail: milos.toth@fei.com.
† FEI Company.
‡ Microstructural Analysis Unit, University of Technology.
§ National Institute of Standards and Technology.
|| Certain commercial equipment is identified in this report to adequately describe the experimental procedure. Such identification does not imply recommendation or endorsement by the National Institute of Standards and Technology, nor does it imply that the equipment identified is necessarily the best available for the purpose. The portion of the work contributed by the National Institute of Standards and Technology is not subject to copyright.

10.1021/nl062848c CCC: $37.00
Published on Web 01/11/2007

cross-talk between interconnects grown by EBID[7]). Furthermore, EBID is often impaired by charging of substrates or deposits that cannot dissipate the charge created by the electron beam. Charging causes defocusing and deflection of the beam, which lead to distortion and lower resolution of the EBID structures.

Here we demonstrate a two-step SEM process capable of producing high-resolution nanostructures, which overcomes problems caused by charging and delocalized deposition. First, ultra-high-resolution environmental SEM (ESEM)[8] is used for EBID of structures such as nanowires and nanopillars. Then, the deposits are slimmed by ESEM imaging in the presence of a second gas which acts as an EBIE precursor for the deposited material but which does not etch the substrate. During EBIE, the ESEM imaging signal[9] provides direct visual feedback of the slimming process, the rate of which can be controlled using the beam current density and the pressure of the EBIE precursor. The minimum achievable feature size is limited by ESEM image resolution (similar to 1 nm,[8] under optimized conditions) and by surface roughening occurring during EBIE.

In the present work, deposition and etching were done using styrene and H_2O precursors. However, the approach presented is applicable to any system in which the EBIE precursor gives rise to etching of structures produced by EBID but which does not etch the substrate. Charging artifacts were eliminated by the use of ESEM[9] for both the deposition and etch processes. The effectiveness of this approach is demonstrated by the use of bulk SiO_2 substrates which charge severely in high-vacuum SEM.

Experiments were performed using an FEI Nova NanoSEM and a similar ESEM system with a gas delivery system modified to permit the mixing and injection of precursors used for EBIE and EBID. Secondary electron imaging was done using a magnetic-field-enhanced gas cascade detector described elsewhere.[10] Briefly, the detector uses an environmental background gas (typically 10−200 Pa of H_2O) to generate a gas ionization cascade. The cascade amplifies the electron imaging signal and generates gaseous ions which are used to stabilize charging of the substrate.[9] EBID of carbonaceous structures was performed using a mixture of styrene ($C_6H_5CH{=}CH_2$) and N_2. The gases were delivered to the specimen chamber simultaneously. Flow rates were controlled using needle valves. First, the N_2 flow control valve was adjusted to achieve a steady-state specimen chamber pressure of ∼22.5 Pa, the pressure needed to stabilize charging[8,9] of the substrates used (single crystal, *z*-cut, 0.5 mm thick SiO_2). Then, the styrene flow control valve was opened so as to increase the total pressure (P) to ∼26 Pa. The resulting gas mixture permitted EBID, while performing the conventional function of an ESEM imaging gas (i.e., elimination of charging artifacts to the extent needed for high-resolution imaging and gas cascade amplification of the electron imaging signal).

During EBID, the accelerating voltage (V_0) was fixed at 30 kV. The electron beam was normal to the sample surface. EBID of nanowires was done by scanning the beam in one dimension, using a dwell time (t_D) of 16.7 ms/line. To perform EBIE, the styrene/N_2 mixture was evacuated and replaced with H_2O. During EBIE, P, V_0, I_0, and t_D were in the range of 60−81 Pa, 10−30 kV, 77−446 pA, and 3−6 μs/pixel, respectively. Sample tilt used during EBIE (i.e., the angle between the target surface and the plane normal to the beam axis) is denoted by ϕ in figure captions. Selected captions show the EBID time (t) and the specific parameters used to fabricate nanostructures.

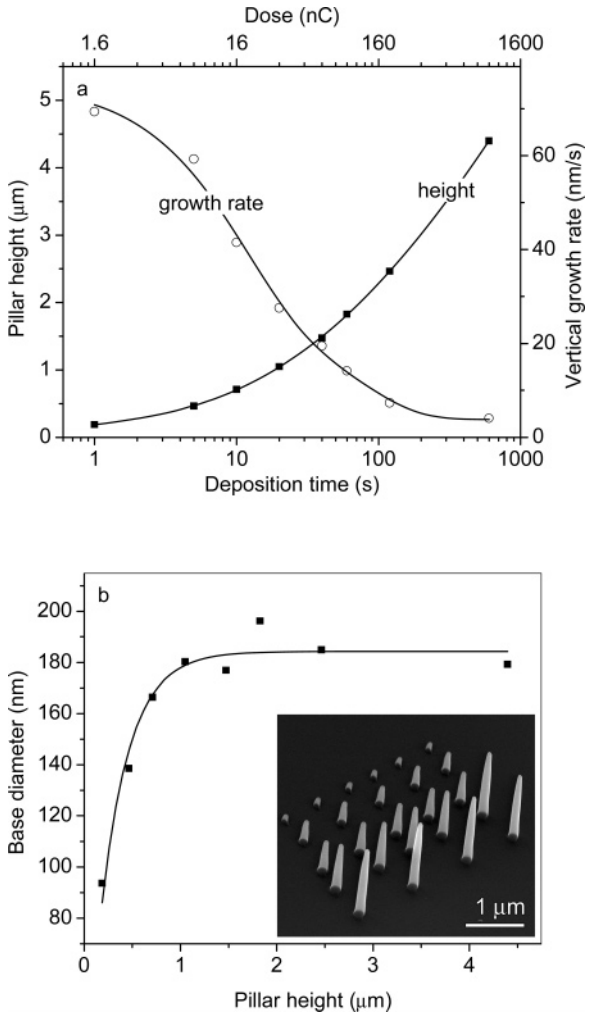

Figure 2. (a) Height and vertical growth rate of carbonaceous pillars grown on bulk SiO_2 using a stationary electron beam, as a function of deposition time. (b) Pillar base diameter as a function of height. Inset: Pillars fabricated using deposition times of 1, 5, 10, 20, and 40 s. $I_0 = 1.6$ nA.

We start by investigating the growth kinetics of carbonaceous pillars deposited on bulk SiO_2 using a stationary electron beam in a styrene/N_2 atmosphere (Figure 2). The pillar vertical growth rate decreased from ∼70 nm/s (∼44 nm/nC, 1 s deposition time) to a steady-state value of ∼3.8 nm/s (∼2.4 nm/nC) (Figure 2a). Initially, the base diameter increased with deposition time and saturated at ∼184 nm (Figure 2b). These growth kinetics are similar to those reported for conventional, high-vacuum EBID on conductive substrates,[11−14] indicating that they are not altered significantly by the low-vacuum environment or by charging of the SiO_2 substrate. This is ascribed to the use of a relatively low pressure (∼22.5 Pa) of an inert ESEM gas (ESEM

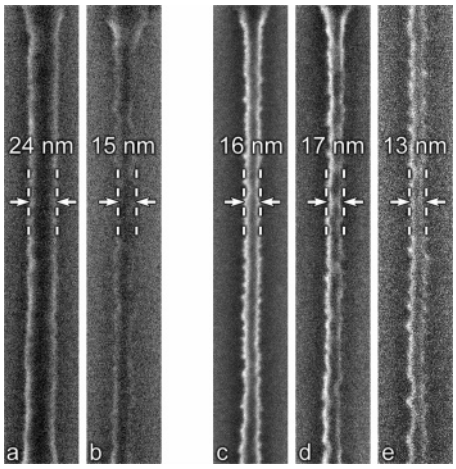

Figure 3. Carbonaceous nanowires fabricated by EBID on a bulk SiO_2 substrate. (a, b) Two frames of a H_2O etch process used to slim the wire in (a) (deposition, $t = 60$ s, $I_0 = 400$ pA; etch, $P = 81$ Pa, $V_0 = 15$ kV, $I_0 = 77$ pA, $t_D = 6$ μs/pixel, $\phi = 0°$). (c−e) Similar nanowires slimmed to produce diameters in the range of 13−17 nm.

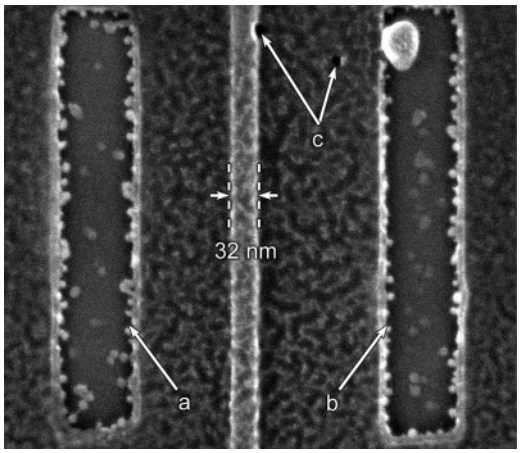

Figure 4. A carbonaceous film and a nanowire fabricated by EBID on a SiO_2 substrate. (a−c) Pits pre-etched into the carbonaceous film using a scanned (a, b) and a stationary (c) electron beam. $\phi = 0°$.

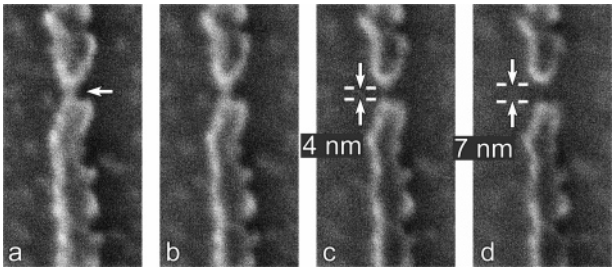

Figure 5. Four consecutive frames of a H_2O EBIE process used to slim a carbonaceous nanowire and to produce the gap shown in (c, d). Gap growth was initiated by a stationary electron beam etch process (~1 s) in the region indicated in (a). (deposition, $t = 30$ s, $I_0 = 0.4$ nA; etch, $P = 60$ Pa, $V_0 = 15$ kV, $I_0 = 77$ pA, $t_D = 3$ μs/pixel, $\phi = 25°$.)

permits the use of gas pressures in excess of 2.5 kPa),[9] a relatively high electron beam energy of 30 keV, and a magnetic-field-assisted gas cascade detector[8,10] capable of stabilizing charging at low gas pressures. Charge control stability is confirmed by the image in the inset of Figure 2b, showing pillars free from distortions caused by charging of the substrate.

We now turn to the process of slimming of EBID structures by EBIE. Figure 3a,b shows two frames of a H_2O etch process used to slim a carbonaceous nanowire on a bulk SiO_2 substrate (the wire was grown by EBID, by scanning the electron beam in one dimension repeatedly for 60 s in a styrene/N_2 atmosphere). The image in Figure 3b was obtained after the wire in Figure 3a was imaged five times in a H_2O atmosphere, causing the nanowire diameter to decrease from approximately 24 to 15 nm. We attribute this slimming primarily to H_2O-mediated EBIE of carbon.[2,15−18] The decrease in nanowire width is driven largely by secondary electrons emitted from the wire sidewalls during imaging. These electrons also give rise to the edge highlighting that produces the image contrast seen in Figure 3. Images c−e in Figure 3 show similar nanowires slimmed to yield diameters in the range of 13−17 nm (the wires shown are physically continuous, and the edge roughness seen in the images is discussed below).

The morphology of structures produced by EBID can also be controlled by pre-etching pits into deposits such as those shown in Figure 4. The image shows a carbonaceous film (filling the entire field of view) and a nanowire fabricated by EBID on a SiO_2 substrate. The EBID structure contains pits that were prefabricated by EBIE using a scanned (a and b) and a stationary (c) electron beam. Subsequent ESEM imaging of these pits (in a H_2O environment) causes them to grow laterally, due to EBIE driven by electrons emitted from the pit sidewalls.

The combination of pre-etching and subsequent EBIE and the visual feedback provided by live ESEM imaging can be used to fabricate nanostructures with a high level of control. This is illustrated by the fabrication of a gap in the carbonaceous nanowire shown in Figure 5. The nanowire was produced by EBID on a bulk SiO_2 substrate. Then, the wire was imaged in a H_2O environment until its width decreased to approximately 20 nm. Next, the pit shown in Figure 5a was etched into the wire sidewall using a stationary electron beam (~1 s irradiation). Finally, the wire was imaged until the pit shown in part a evolved into the gap shown in parts c and d. The images in Figure 5 are the last four frames of this slimming process. We note that such high-resolution real-time monitoring is not achievable by high-vacuum SEM. Nanoscale etch processes dynamically alter local charging behavior, creating the need for a charge control mechanism that does not affect the electron beam or the imaging signal. In high-vacuum low-voltage SEM, charge control self-regulation is achieved through modulation of the secondary electron yield and the electron beam landing energy,[19] leading to quenching of the imaging signal and image distortion caused by defocusing and deflection of the electron beam. Conversely, in ESEM, self-regulation is achieved through modulation of the ion current impinging on the sample surface,[8] permitting high resolution, artifact-

free imaging of dynamically evolving structures on insulating substrates, such as the nanowire-on-SiO_2 shown in Figure 5.

Etch processes such as that used to create the gap shown in Figure 5 can be terminated by blanking the electron beam once the desired feature morphology is observed in an image. During imaging, the EBIE rate is governed by sample temperature, beam energy, and current density (determined by the current, magnification, and dwell time) and the pressure of the gaseous precursor. These parameters provide a high level of control over the EBIE rate during imaging. For example, in general, the etch rate decreases with increasing temperature and decreasing current density, as in high-vacuum EBIE and EBID,[1,13,14,20] and an increase in precursor partial pressure raises the current density at which the growth rate transitions from being limited by the reaction rate to being limited by mass transport of the precursor.[1,21] An increase in electron beam landing energy (E_0) serves to reduce the etch or deposition rate (provided $E_0 > \sim 100$ eV)[1,13,22−24] due to the energy dependence of dissociation cross sections. However, at the relatively high pressures permissible in ESEM (>2 kPa),[9] the role of pressure and beam energy is complicated by scattering of beam electrons in the gas. Scattered electrons form a diffuse "skirt" around a focused beam component.[25,26] The electron mean-free path (λ) decreases with increasing pressure and decreasing energy. A decrease in λ causes a decrease in beam current density,[25] which serves to reduce the etch rate under the electron beam. Hence, the net dependence of EBIE rate on beam energy and pressure is governed by the energy dependencies of cross sections for electron scattering and precursor dissociation.

In practice, the above parameters must be optimized for ESEM imaging and charge control.[9,10,27] This can result in undesirable process behavior (e.g., an etch rate that is too high for effective end-pointing by high-resolution ESEM imaging). However, such problems can be overcome using a mixture of a chemically inert ESEM imaging gas (e.g., N_2) and the EBIE precursor (e.g., H_2O or XeF_2). The simultaneous ESEM imaging and EBIE process described here permits rapid characterization of EBIE rates as a function of parameters such as the partial pressures of different etch precursors.

The pre-etching and subsequent EBIE illustrated in Figures 4 and 5 can also be used to remove delocalized deposits produced during EBID. Delocalized deposits are typically grown unintentionally due to backscattering of incident beam electrons from the substrate, emission of backscattered electrons from deposit sidewalls (and subsequent impact at the sample surface), and beam scatter in the gas surrounding the target. The latter can be particularly problematic in ESEM which permits the use of high gas pressures (>2.5 kPa) and where delocalized EBID is enhanced by molecules activated in the gas cascade. A cleanup etch process, such as that discussed here, is therefore highly desirable in EBID done using environmental as well as conventional SEM.

We now turn to the process of surface roughening which occurs during EBIE. Figure 6a shows a carbonaceous pillar grown by EBID. The pillar tip was slimmed by ESEM

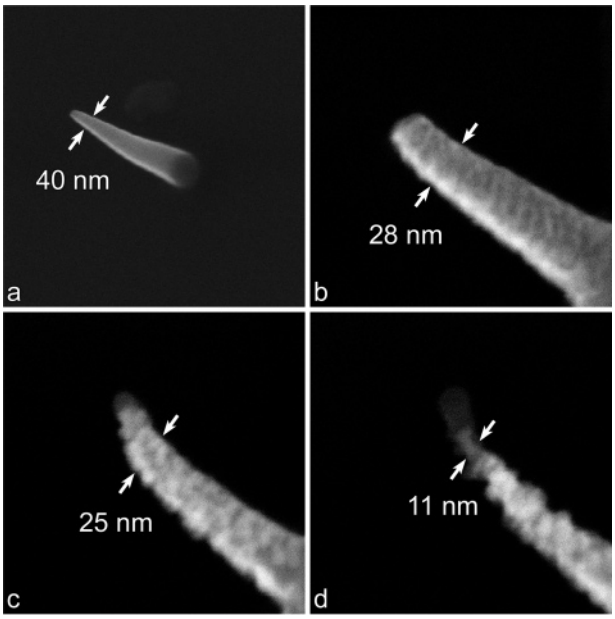

Figure 6. (a) Carbonaceous pillar grown on bulk SiO_2 using a stationary electron beam. (b-d) Frames 1, 42, and 90 of a H_2O etch process used to etch the pillar shown in (a). (deposition, $t = 20$ s, $I_0 = 0.4$ nA; etch, $P = 60$ Pa, $V_0 = 15$ kV, $I_0 = 77$ pA, $t_D = 3$ μs/pixel, $\phi = 25°$.)

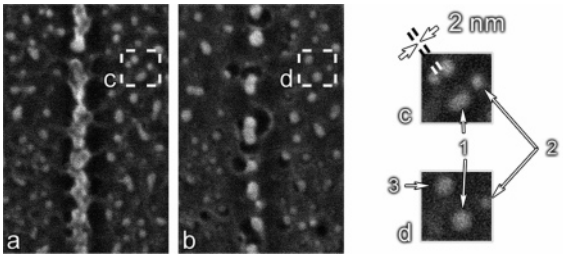

Figure 7. (a) A frame from an ESEM imaging EBIE process of a carbonaceous film and a nanowire (prefabricated by EBID on a SiO_2 substrate). (b) The same region, imaged after an additional five frames of EBIE. (c, d) Digitally enlarged detail from images (a) and (b). (deposition, $I_0 = 0.4$ nA; etch, $P = 80$ Pa, $V_0 = 30$ kV, $I_0 = 446$ pA, $t_D = 6$ μs/pixel, $\phi = 0°$.)

imaging in a H_2O environment. Images b−d show frames 1, 42, and 90 of this EBIE process. The images illustrate surface roughening that is often observed during EBIE.[24,28] Such roughening alters and can dominate the morphology of structures produced by EBIE. This is illustrated further in Figure 7 by images of a partially etched carbonaceous film (that originally filled the entire field of view) and a nanowire fabricated by EBID. Images a and b are two frames of an ESEM imaging process used to etch the wire and the film. The film is highly irregular and contains structure, enlarged in (c) and (d), which developed during etching. We note that the distance between features 1 and 2 increased, while the other two features seen in (c) merged into feature 3 during EBIE. Features such as 1, 2, and 3 were observed to exhibit lower EBIE rates than the surrounding carbonaceous film despite their higher secondary electron yields. This behavior indicates chemical modification and densification of the carbonaceous film during EBIE. This is ascribed to electron-induced modification of carbonaceous material,

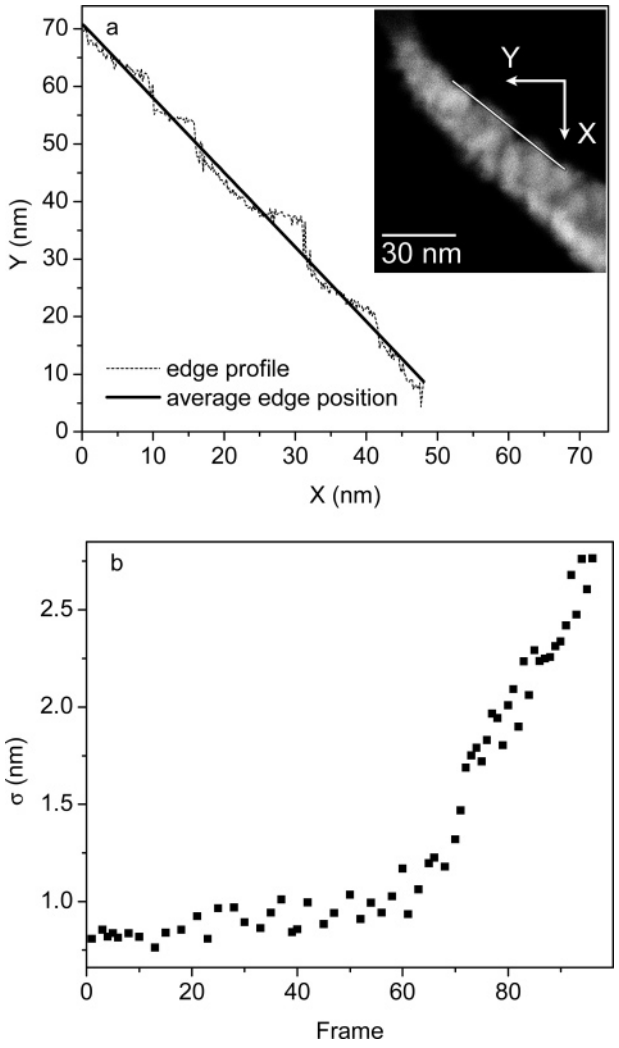

Figure 8. (a) Edge profile obtained from frame 80 (shown in the inset) of the etch process shown in Figure 6 and the corresponding average edge position. The inset shows the edge analyzed, and the *X* and *Y* coordinates used in (a). (b) Edge roughness (σ) as a function of frame number.

driven by processes such as H−C bond cracking, high order (C═C and C≡C) carbon−carbon bond formation, and H desorption from the film.[29,30] The extent of the resulting surface roughening is a function of parameters such as deposit thickness, electron beam energy, and current density (for example, the gross structure seen in Figure 7 was obtained by using a relatively high beam current and energy of 446 pA and 30 keV).

We can quantify the edge roughness (σ) of deposits using

$$\sigma = \sqrt{\frac{1}{N}\sum_{i=1}^{N} \delta_i^{\,2}} \qquad (1)$$

where N is the number of pixels along an edge and δ is the distance of each edge point from a linear fit of the edge position.[31] Figure 8a shows an edge profile obtained from frame 80 of the pillar etch process shown in Figure 6 and the corresponding average edge position. The edge roughness exhibits a complex dependence on etch time (Figure 8b), attributed to the competing effects of electron irradiation on etch rate. Surface roughening causes an increase in secondary electron yield, which accelerates the etch rate. However, electron irradiation also causes the above-mentioned chemical modification of the deposit, leading to the formation of regions (e.g., features 1−3 shown in Figure 7) of locally reduced etch rate. The competition between these processes gives rise to complex etch kinetics that are a function of the initial deposit volume and composition. The details of the roughening process are the subject of ongoing studies where EBID and EBIE processes are being applied to the fabrication of structures such as metallic interconnects.

Finally, we note that the composition of carbonaceous deposits produced using a wide range of hydrocarbon precursors has been reported to consist of amorphous carbon (typically containing more sp^2 than sp^3 bonds), oxygen, and hydrogen and the deposit composition to be relatively independent of that of the precursor.[30,32−34] Hence, the electron-beam-induced modification processes discussed above are expected to play the dominant role in the final composition and uniformity of the deposits shown in Figure 3, 5, 6, and 7.

In summary, we have described a sequential EBID−EBIE nanofabrication methodology which can decrease the minimum dimensions of EBID structures, is not limited by charging, and provides a means for the removal of thin films produced unintentionally during EBID.

References

(1) See, for example, the recent review by: Randolph, S. J.; Fowlkes, J. D.; Rack, P. D. *Crit. Rev. Solid State Mater. Sci.* **2006**, *31* (3), 55−89.
(2) Folch, A.; Tejada, J.; Peters, C. H.; Wrighton, M. S. *Appl. Phys. Lett.* **1995**, *66* (16), 2080−2082.
(3) Molhave, K.; Madsen, D. N.; Dohn, S.; Boggild, P. *Nanotechnology* **2004**, *15* (8), 1047−1053.
(4) Tanaka, M.; Shimojo, M.; Han, M.; Mitsuishi, K.; Furuya, K. *Surf. Interface Anal.* **2005**, *37* (2), 261−264.
(5) van Dorp, W. F.; van Someren, B.; Hagen, C. W.; Kruit, P. *Nano Lett.* **2005**, *5* (7), 1303−1307.
(6) Guise, O.; Ahner, J.; Yates, J.; Levy, J. *Appl. Phys. Lett.* **2004**, *85* (12), 2352−2354.
(7) Gopal, V.; Stach, E. A.; Radmilovic, V. R.; Mowat, I. A. *Appl. Phys. Lett.* **2004**, *85* (1), 49−51.
(8) Toth, M.; Knowles, W. R.; Thiel, B. L. *Appl. Phys. Lett.* **2006**, *88* (2), 023105.
(9) See, for example, the recent review by Thiel, B. L.; Toth, M. *J. Appl. Phys.* **2005**, *97* (5), 051101.
(10) Thiel, B. L.; Toth, M.; Schroemges, R.; Scholtz, H.; G., v. V.; Knowles, W. R. *Rev. Sci. Instrum.* **2006**, *77* (3), 033705.
(11) Kohlmann-von, Platen, K. T.; Chlebek, J.; Weiss, M.; Reimer, K.; Oertel, H.; Brunger, W. H. *J. Vac. Sci. Technol., B* **1993**, *11* (6), 2219−2223.
(12) Bret, T.; Utke, I.; Bachmann, A.; Hoffmann, P. *Appl. Phys. Lett.* **2003**, *83* (19), 4005−4007.
(13) Beaulieu, D.; Ding, Y.; Wang, Z. L.; Lackey, W. J. *J. Vac. Sci. Technol., B* **2005**, *23* (5), 2151−2159.
(14) Randolph, S. J.; Fowlkes, J. D.; Rack, P. D. *J. Appl. Phys.* **2005**, *97* (12), 124312.
(15) A discussion of early work on etching of carbonaceous films can be found in the review by: Hern, J. J. Barriers to AEM: Contamination and etching. In *Introduction to analytical electron microscopy*; Hern, J. J., Goldstein, G. I., Joy, D. C., Eds.; Plenum Press: New York, 1979; pp 481−505.
(16) Wang, D.; Hoyle, P. C.; Cleaver, J. R. A.; Porkolab, G. A.; Macdonald, N. C. *J. Vac. Sci. Technol., B* **1995**, *13*(5), 1984−1987.
(17) Kohlmann-von, Platen, K. T.; Bruenger, W. H. *J. Vac. Sci. Technol., B* **1996**, *14* (6), 4262−4266.

(18) Molhave, K.; Madsen, D. N.; Rasmussen, A. M.; Carlsson, A.; Appel, C. C.; Brorson, M.; Jacobsen, C. J. H.; Boggild, P. *Nano Lett.* **2003**, *3* (11), 1499−1503.
(19) See, for example: Cazaux, J. *Scanning* **2004**, *26* (4), 181−203, and references therein.
(20) Li, W.; Joy, D. C. *J. Vac. Sci. Technol., A* **2006**, *24* (3), 431−436.
(21) Fowlkes, J. D.; Randolph, S. J.; Rack, P. D. *J. Vac. Sci. Technol., B* **2005**, *23* (6), 2825−2832.
(22) Hoyle, P. C.; Cleaver, J. R. A.; Ahmed, H. *Appl. Phys. Lett.* **1994**, *64* (11), 1448−1450.
(23) Hoyle, P. C.; Cleaver, J. R. A.; Ahmed, H. *J. Vac. Sci. Technol., B* **1996**, *14* (2), 662−673.
(24) Rack, P. D.; Randolph, S.; Deng, Y.; Fowlkes, J.; Choi, Y.; Joy, D. C. *Appl. Phys. Lett.* **2003**, *82* (14), 2326−2328.
(25) Moncrieff, D. A.; Barker, P. R.; Robinson, V. N. E. *J. Phys. D, Appl. Phys.* **1979**, *12* (4), 481.
(26) Danilatos, G. D.; Phillips, M. R.; Nailon, J. V. *Microsc. Microanal.* **2001**, *7* (5), 397−406.
(27) Thiel, B. L. *Ultramicroscopy* **2004**, *99* (1), 35−47.
(28) Randolph, S. J.; Fowlkes, J. D.; Rack, P. D. *J. Appl. Phys.* **2005**, *98* (3), 034902.
(29) Vesely, D. *Ultramicroscopy* **1984**, *14* (3), 279−290.
(30) Guise, O.; Marbach, H.; Levy, J.; Ahner, J.; Yates, J. T. *Surf. Sci.* **2004**, *571* (1−3), 128−138.
(31) See, for example: Patsis, G. P.; Constantoudis, V.; Tserepi, A.; Gogolides, E.; Grozev, G. *J. Vac. Sci. Technol., B* **2003**, *21* (3), 1008−1018.
(32) Miura, N.; Yamada, A.; Konagai, M. *Jpn. J. Appl. Phys., Part 2: Lett.* **1997**, *36* (9AB), L1275−L1278.
(33) Bret, T.; Mauron, S.; Utke, I.; Hoffmann, P. *Microelectron. Eng.* **2005**, *78*−*79*, 300−306.
(34) Ding, W.; Dikin, D. A.; Chen, X.; Piner, R. D.; Ruoff, R. S.; Zussman, E.; Wang, X.; Li, X. *J. Appl. Phys.* **2005**, *98* (1).

NL062848C